Title
SERS optical fiber probe with plasmonic end-facet

Journal
Journal of Raman Spectroscopy, 48(2)

ISSN
0377-0486

Authors
Xia, Ming
Zhang, Pei
Leung, Claris
et al.

Publication Date
2017-02-01

DOI
10.1002/jrs.5031

Peer reviewed

Research article

Journal of RAMAN SPECTROSCOPY

Received: 20 April 2016 Revised: 18 August 2016 Accepted: 20 August 2016 Published online in Wiley Online Library: 14 September 2016

(wileyonlinelibrary.com) DOI 10.1002/jrs.5031

SERS optical fiber probe with plasmonic end-facet

Ming Xia,[a]* Pei Zhang,[a] Claris Leung[a] and Ya-Hong Xie[a,b]

Surface-enhanced Raman spectroscopy (SERS) is a surface-sensitive technique that can enhance the intensity of Raman signal by several orders of magnitude, enabling even the detection of single molecule. This work presents the experimental and theoretical studies of an optical fiber probe with nano-structured end-facet for bio-sensing applications via SERS. The factors affecting the intensity of Raman signal passing through the fiber probe are investigated. These factors include the numerical aperture of the objective lens, the slit width of the spectrometer, the fiber length, and the size of SERS nano-array. The Raman signal loss through fiber compared with optical microscope-based free-space Raman detection is estimated. To further enhance the SERS enhancement factor, a hybrid graphene/Au nano-triangle structure is transferred on the end-facet of the fiber probe to enable SERS. Superimposing graphene layer on Au nano-structure is found to be superior over bare Au nano-structure in terms of the detection sensitivity. Copyright © 2016 John Wiley & Sons, Ltd.

Additional supporting information may be found in the online version of this article at the publisher's web site.

Keywords: SERS; optical fiber; graphene

Introduction

Surface-enhanced Raman spectroscopy (SERS) is an important analytical technique that is able to provide single molecule detection and high-resolution spectral information.[1] It is capable of single molecule detection and allows for label-free detection with high degree of specificity.[2] Molecules absorbed at the metallic surface experience a large amplification of the electromagnetic field because of local surface plasmon resonance leading to orders of magnitude increase in Raman yield and greatly enhanced Raman signal. To achieve high SERS enhancement factors (EFs), many efforts have been devoted to develop various metallic (mainly Au and Ag) nano-structures to enhance the local electromagnetic field.[3–5] In addition to the traditional metallic nano-structures, graphene and other two-dimensional materials have also been explored to enhance the Raman signal.[6–9] SERS has been explored for *in vivo* tumor detection with labeled Au nanoparticles,[10,11] in which the specificity of detection is enabled by labeling technique. Compared with labeled nanoparticles, SERS optical fiber probe with single-ended measurement geometry[12–19] has been gaining attention for *in vivo* label-free bio-sensing because of their flexibility and compatibility with remote sensing. A label-free detection scheme allows real-time detection and eliminates the time and cost-consuming labeling procedures.[20] Moreover, label-free SERS renders vibrational information akin to fingerprints of the biomolecules that is in principle more specific than any labeling approaches. The most common method to couple SERS substrates with optical fiber is to modify the fiber end with SERS substrates such as Ag or Au nanoparticles.[14–16,21] Nanoparticle-coated optical fiber probe for *in vitro* SERS measurement[14,16] can achieve EF on the order of 10^4–10^5, lower than the common single molecule SERS EF of ~10^7–10^8.[2] SERS fiber probes prepared using this method have spatial resolution similar to the fiber core diameter (usually larger than 10 μm). However, higher spatial resolution is demanded in certain bio-sensing, like *in vivo* neurochemical monitoring.[22] For instance, measurement of neurodynamics within individual synaptic clefts (tens of nanometers[23]) represents the most extreme challenge. To expand the SERS fiber probe for *in vivo* bio-sensing, optimization of SERS fiber probe is required to provide higher SERS EF and spatial resolution.

The optimization of SERS fiber probe can be achieved only if the key factors affecting the sensitivity are well understood. This paper describes our effort in gaining such understanding. We prepare SERS fiber probes based on Au nano-triangle array and propose a method to enhance its spatial resolution. The key factors studied here include the numerical aperture (NA) of objective lens, the slit width of spectrometer, the fiber length, and the size of SERS nano-array. The Raman signal loss through the fiber is estimated compared with normal Raman detection. To further enhance the SERS EF, a hybrid graphene/Au nano-triangle structure is transferred on fiber facet. SERS fiber probe with hybrid graphene/Au nano-triangle structure is found to have better performance than the fiber probe with bare Au nano-triangle structure.

Methods

The SERS fiber probe is prepared by transferring Au nano-triangle array onto the fiber facet. The fabrication process is shown in Fig. S1. SERS measurement is conducted using Renishaw inVia confocal Raman microscope with 785 nm laser (12.5 mW power with 20 s

* *Correspondence to: Ming Xia, Department of Materials Science and Engineering, University of California Los Angeles, Los Angeles, CA 90095, USA. E-mail: xiaming@g.ucla.edu*

a *Department of Materials Science and Engineering, University of California, Los Angeles, Los Angeles, CA, 90095, USA*

b *Jonsson Comprehensive Cancer Center, University of California, Los Angeles, Los Angeles, CA, 90095, USA*

accumulation time). The SERS optical fiber is coupled to the microscope using a homemade fiber holder. Figure 1(a) shows the schematic diagram of the experiment setup. Rhodamine 6G (R6G) is used as analyte molecule. Unless otherwise stated, the R6G Raman data are measured in liquid solution in the following experiment. Scanning electron microscope image in Fig. 1(b) shows the Au nano-triangle array transferred on the fiber end.

Results and discussion

We first consider the effect of the NA of the objective lens on the Raman signal. Figure 2(a) shows the Raman spectra measured from the same SERS fiber probe with different objective lens. Figure 2(b) shows the reference Raman spectrum of SERS fiber without R6G. The slit width of the spectrometer is chosen as 300 μm for all three lenses to make sure all the Raman-shifted light coming out of near end of fiber can be collected by spectrometer. The highest Raman signal intensity is achieved by 20× lens with 0.4 NA, followed by 50× lens with 0.75 NA. Five characteristic Raman peaks of R6G, 1311, 1360, 1507, 1595, and 1648 cm^{-1}, can be distinguished clearly using 20× lens. Raman signal obtained from 50× lens has lower intensity than that from 20× lens, but the R6G peaks are still discernible. However, Raman spectrum obtained from 5× lens does not show any discernible R6G peaks. For a given SERS fiber probe with analyte molecules on its far end, Raman signal intensity (S) obtained through the fiber can be expressed as follows:

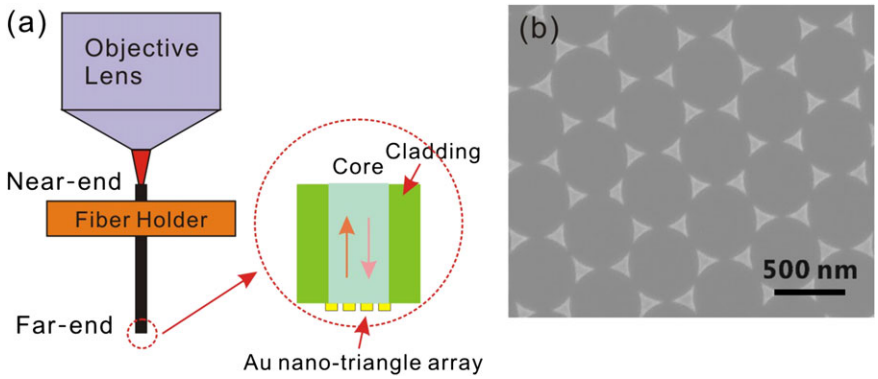

Figure 1. (a) Schematic diagram of the experiment setup. (b) Scanning electron microscope image of Au nano-triangle array.

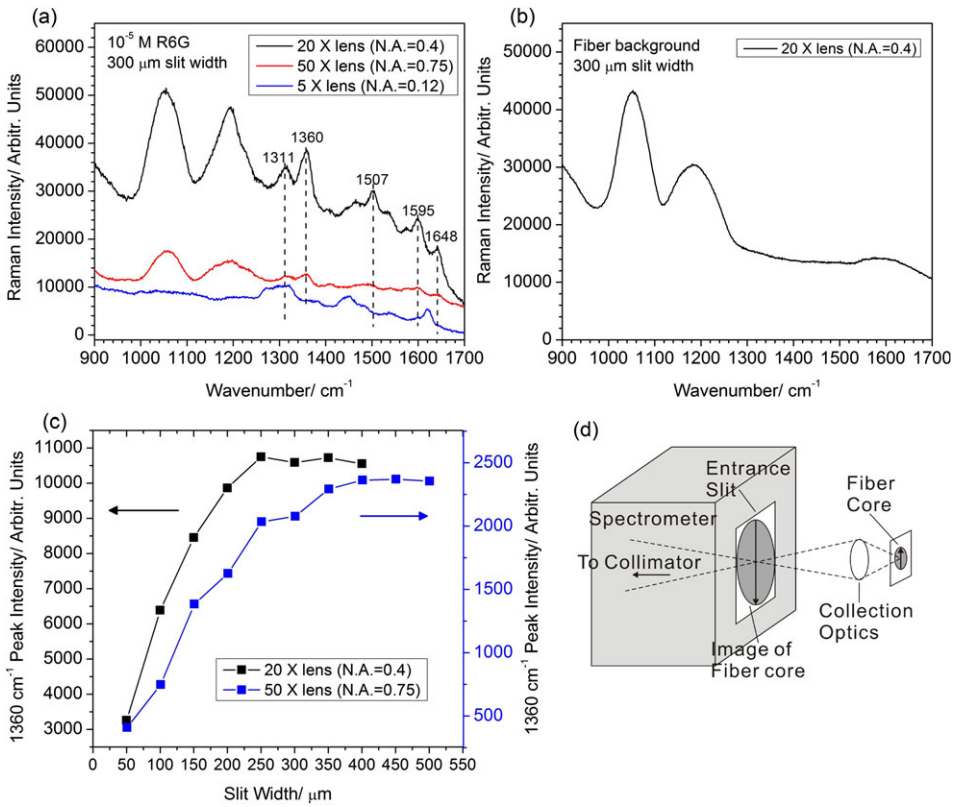

Figure 2. (a) Raman spectra of R6G solution measured with surface-enhanced Raman spectroscopy fiber probe (11 cm long) using different lens. (b) Reference Raman spectrum of surface-enhanced Raman spectroscopy fiber without R6G. (c) Dependence of R6G peak intensity on spectrometer slit width. (d) Illustration of fiber-to-spectrometer matching.[24]

$$S \propto I_0 \times a \times b$$

Where I_0 is incident laser power on the near end of fiber, a is the coefficient representing the percentage of laser power that coupled into the fiber, and b is another coefficient representing the percentage of Raman signal coming out of the fiber (near end) that collected by the objective lens. The precondition for this expression is that laser-focused spot size is smaller than that of fiber core. For 5×, 20×, and 50× lens, the R6G 1360 cm^{-1} peak intensity as seen in Fig. 2(a) are about 0, 10,000, and 2000 counts, respectively. This can be reconciled with the expected values based on the consideration that $(a\ \ b) = (0.22 / NA_{lens})^2$. The calculated value (0.302) for 20× lens is about four times of that value (0.085) for 50× lens, which is in reasonable agreement with the experimental result. The only noticeable difference is for 5× lens, which could be explained by that the laser-focused spot size for 5× lens is larger than the fiber core, and therefore, laser power coupled into fiber also decreases ($a < 1$). The combination of the two factors ($a < 1$ and $b = (0.22 / NA_{lens})^2$) causes the Raman signal intensity with 5× lens the lowest. Based on the previous discussion, higher Raman signal can be achieved when the NA of the objective lens is close to or match the NA of the fiber, assuming other conditions are the same.

The next factor affecting the Raman signal is the slit width of the spectrometer. The Raman signal intensity dependence on the slit width is shown in Fig. 2(c), where R6G 1360 cm^{-1} peak intensity is used as a metric of Raman signal intensity. By increasing the slit width from 50 to 400 μm, Raman signal increased by ~200% for 20× lens while background noise increased by ~20%. Thus, widening the slit actually improves the signal to noise ratio (S/N). The trend continues up till the slit width reaches saturation point (~250 μm for 20× lens). The reason is that beyond that saturation point, the signal stops increasing with noise continues going up, making the ~250 μm width the optimum for S/N. The optimum value is dependent on NA of the lens, and it is 400 μm for 50× lens. This can be understood as follows. When the Raman signal from the near end of the fiber comes into the objective lens and is collected by the spectrometer, the image of fiber core is projected on the slit of spectrometer, as shown in Fig. 2(d). If the magnified fiber core image size is larger than the slit width, a part of the Raman signal does not enter into the spectrometer. When the magnified fiber image just matches the slit width, the Raman signal intensity reaches the maximum. Further increasing the slit width will not help enhance the signal intensity but increase the stray light and cause noise. For 20× lens, Raman signal saturates at ~250 μm slit width, which means the core image is enlarged for about five times at slit width. The magnification for 50× lens is larger than 20×, so the enlarged fiber core image on the slit is also larger, and thus, the signal should saturate at larger slit width. Therefore, by increasing the slit width within certain range, Raman signal intensity can be enhanced. In the following Raman measurement, 20× lens and a slightly higher slit width (300 μm) is used in order to collect all the Raman light.

To study how fiber length affects Raman signal intensity, we investigated the S/N of R6G Raman peak and the noise dependence on the fiber length. R6G 1360 cm^{-1} peak is chosen to calculate the S/N. As shown in Fig. 3(a), the S/N changes from about 5 for 400-cm-long fiber to about 11 for 3-cm-long fiber, increasing by about two times. The noise changes from about 2000 counts for 400-cm-long fiber to about 800 counts for 3-cm-long fiber, decreasing by about two times. We notice that the error bars of S/N ratio are large for fiber length from 3 to 11 cm. However, there is a clear decrease of S/N as fiber length increases from 3 to 400 cm. Our results indicate that the fiber length indeed plays a role in noise increase, and S/N ratio decreases when fiber length increases from several centimeters to hundreds of centimeters. Figure 3(b) shows the Raman spectra of R6G measured using SERS fiber with different length. As the fiber length increases, the florescence background of fiber keeps increasing. Figure 3(c) indicates the bare fiber background intensity (1053 cm^{-1} broad peak) dependence on fiber length, which shows a linear relationship between background intensity and fiber length within the length scale investigated. It is worth noting that in Fig. 3(b) the R6G Raman peak intensity remains nearly constant as fiber length increases to 200 cm. This observation is consistent with the theoretical calculation based on the fiber attenuation. The attenuation of the fiber used is about 8 dB km^{-1} in the range of 750–800 nm, which means that the Raman signal loss within the fiber is negligible (<0.5%) for fiber less than 5 m. The previous analyses indicate that the increase of the noise mainly comes from the fiber background as fiber length increases, which causes the decrease of the S/N ratio. Therefore, the fiber length is not a primary concern for Raman signal intensity loss within the length scale investigated here, but it will affect the S/N of the Raman spectrum and thus affect the performance of SERS fiber probe. The impact on S/N from the fiber fluorescent background can be partially reduced by increasing the collection time or using long wavelength laser.

As seen in Fig. 4, the Raman signal intensity increases with SERS array area on fiber end. For SERS fiber with Au-triangle array coated on the whole fiber core (50 μm in diameter), the highest Raman signal can be achieved, and the detection limit can reach 10^{-6} M for R6G solution. As SERS array decreases to 10 μm-length square, no

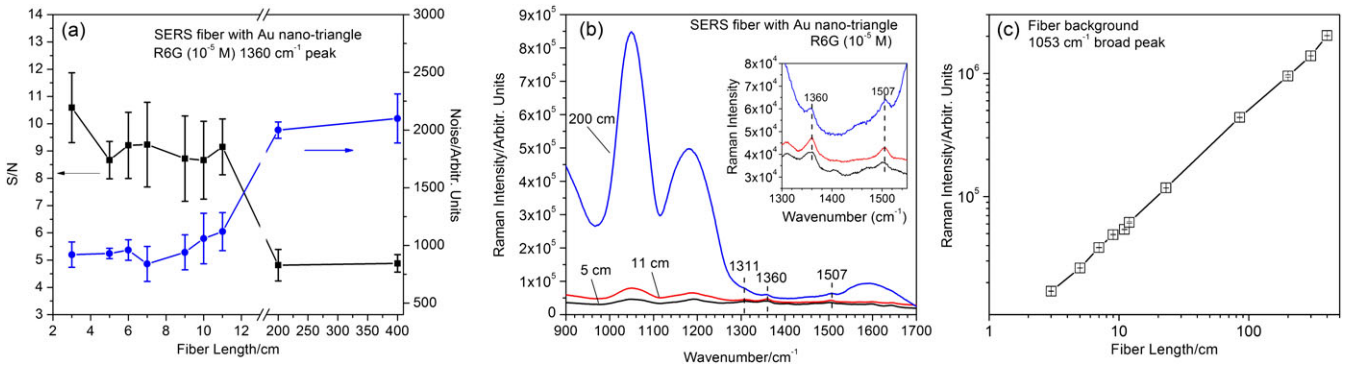

Figure 3. (a) The S/N ratio and the noise dependence on SERS fiber length. (b) Raman spectra of R6G measured using SERS fiber probe with different length (the background of fiber is not removed). The inset figure is the enlarged spectra between 1300 and 1550 cm^{-1}. (c) Fiber background intensity dependence on fiber length.

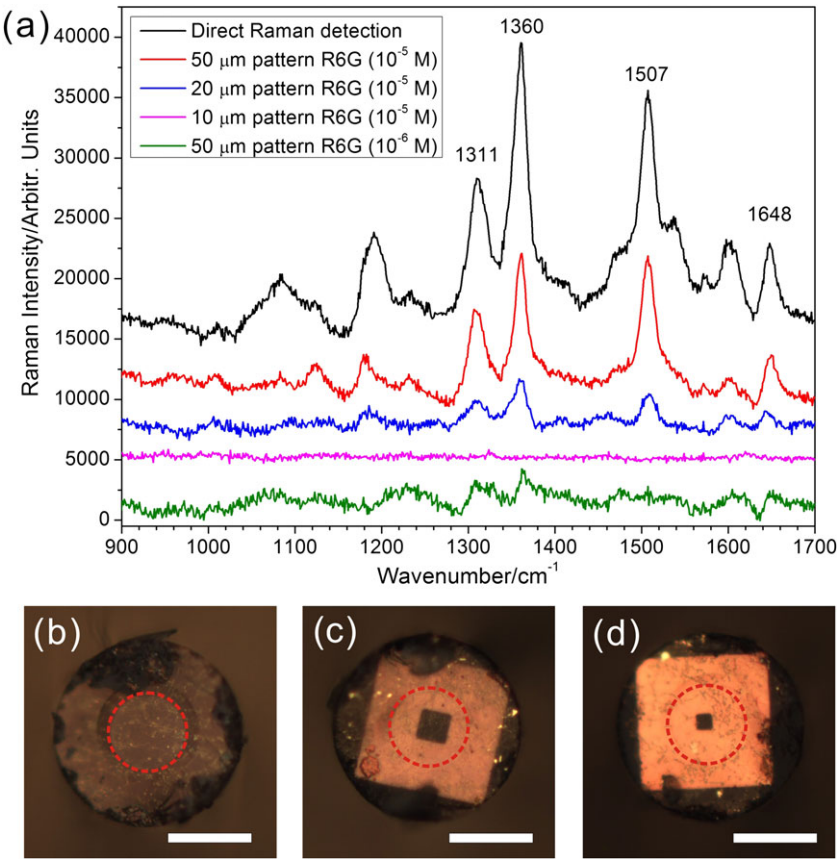

Figure 4. (a) R6G Raman spectra obtained by surface-enhanced Raman spectroscopy fiber probes (11 cm long). Fiber background has been removed in (a). For comparison, R6G spectrum (black curve) measured by the normal detection scheme (Raman signal directly enter into objective lens) is also shown in (a). (b–d) Optical images of fiber probe with Au triangle array covering the whole surface (b), 20 μm Au array (c) and 10 μm Au array (d) covering on fiber core. Scale bar in (b–d) is 50 μm. Red circles indicate the regions of fiber cores.

R6G Raman peak is discernible. The Raman signal increases linearly with SERS array area, and the spatial resolution is proportional to the square root of the area. The results indicate that there is a fundamental trade-off between spatial resolution and signal intensity. Spatial resolution improves with smaller surface area, provided that the signal is still detectable. To achieve higher spatial resolution of the SERS fiber probe, higher SERS EF of the nano-structure is required to compensate for the decrease of the SERS array size.

To estimate the Raman signal loss of the SERS fiber probe compared with direct Raman detection method, Raman measurement of R6G (10^{-5} M) on Au nano-triangle array is conducted. For direct Raman detection, the laser is directly focused on the fiber end with SERS substrates, and the Raman signal is collected by the objective lens. SERS fiber probe used for direct Raman detection is first immersed into R6G solution (10^{-5} M) for 10 min and then dried for measurement. Black spectrum in Fig. 4(a) shows the R6G Raman spectrum measured through the direct detection. Taking R6G 1360 cm^{-1} peak intensity as a metric, Raman signal intensity measured by the direct method is about two times of that measured through fiber probe, indicating that the Raman signal loss due to the fiber is about 50%. When the experimental setup is fixed, Raman signal intensity can be expressed as follows:

$$S \propto \frac{I_0}{A} \times A_D \times D \times \Omega \times t$$

where S is Raman signal intensity expressed in Raman photons, I_0 is incident laser power (photons s^{-1}) shinning on the analyte molecules, A is laser spot area (cm^2), A_D is the sample area monitored by spectrometer (cm^2), D is the molecule density(# cm^{-2}), Ω is the solid angle collected by objective lens (sr), and t is collection time (s). In SERS fiber probe detection method, laser light comes out from 20× objective lens (NA = 0.4) and couples into the fiber (NA = 0.22), in which only 30.25% of laser intensity (I_0) is coupled into the fiber and finally illuminated the molecules on the fiber core. For direct Raman detection, laser spot area (A) is the same as the sample area (A_D) monitored by spectrometer. For the fiber detection, the spectrometer slit width has been enlarged so that the entire fiber core image can entrance the slit, which also means A is equal to A_D. The molecule density D and collection time t are the same for both detection methods. Raman signal coming from laser spot region is collected by 20× lens (NA = 0.4) for the direct detection, but for the fiber detection, Raman signal coming from fiber core region (NA = 0.22) is collected by objective lens. Because of the smaller NA of fiber, the solid angle value for the fiber detection is only 30.25% of that for the direct detection. Based on the previous analysis, the Raman signal measured by fiber method is approximately 10% (30.25% × 30.25%) of that measured by the direct detection, which is comparable with the experimental results (about 50% loss). It is worth noting that laser power density (photos s^{-1} cm^{-2}) at molecules decreases for fiber detection method compared with normal Raman detection, but the larger fiber core area (i.e., larger amount of analyte molecules) compensates for the laser power density decrease. Therefore, to keep the spatial resolution (laser-focused spot size is about 4 μm for 20×

Journal of RAMAN SPECTROSCOPY

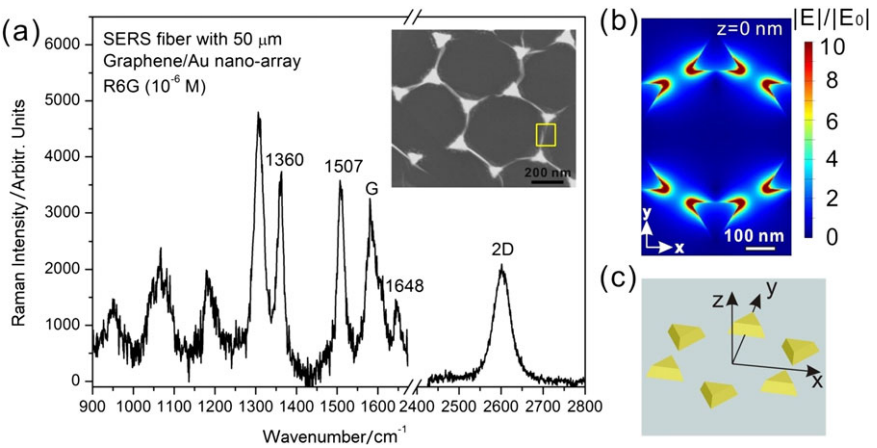

Figure 5. (a) Rhodamine6G (R6G) Raman spectrum obtained by surface-enhanced Raman spectroscopy (SERS) fiber probe with graphene/Au nano-triangle (11 cm long). Inset scanning electron microscope image shows graphene covering on Au nano-triangle. Yellow boxed area indicates the graphene fold formed between neighboring Au triangles. (b) Electrical field magnitude mapping along *x*-*y* plan for $z = 0$ nm. (c) Schematic model of Au triangle array used for FDTD simulation, in which incident light is along *z*-axis and polarization direction is along *x*-axis.

lens) of direct Raman detection, the SERS nano-array size on fiber facet needs to be reduced to the similar size of laser spots. In this situation, laser power density decrease will become the primary factor that contributes to the Raman signal loss. Therefore, SERS nanostructure with higher EF is required to compensate for the laser power density decrease.

To improve EFs of SERS fiber probes, graphene is transferred on Au nano-triangle array on SERS fiber probe [inset image in Fig. 5(a)]. Through superimposing graphene over metallic SERS substrates, higher SERS EF has been obtained for selected families of molecules.[7,25] Graphene as a substrate for enhancing Raman scattering has been reported widely.[6,8,26–28] This enhancement is mainly attributed to the charge transfer between graphene and the molecules, resulting in a SERS chemical enhancement.[26,28] Charge transfer causes the positive and negative charges in the molecule to be more separated, which increases the polarizability of the molecule and then the cross section of the Raman scattering. Charge transfer occurs when the graphene Fermi level is located in between the highest occupied molecular orbital (HOMO) and the lowest unoccupied molecular orbital (LUMO) of molecules including R6G.[7] In our experiment, we did observed this enhancement using graphene/Au hybrid SERS fiber probe, as seen in Fig. 5(a). Graphene 2D and G peaks are readily apparent, and graphene D peak overlaps with R6G 1311 cm^{-1} peak. R6G Raman peak intensities measured by Au/graphene fiber probe are larger than that by the fiber probe with bare Au nano-array for the same concentration of R6G solution (10^{-6} M), which is due to the chemical enhancement of graphene. The introduction of graphene not only enhanced the Raman signal intensity but also would help *in vivo* bio-sensing using SERS fiber probe due to its bio-compatibility and chemical stability.[29–31] Through transferring graphene/Au hybrid substrates on fiber, we have demonstrated that Au triangle/graphene is suitable for fiber-based SERS sensing applications. Although the SERS enhancement for this hybrid SERS substrate is relatively low compared with nanoparticle-based substrates, the substrate has larger SERS-active zones than nanoparticle-based substrates. As shown in the finite-difference time-domain (FDTD)-simulated electric field distribution [Fig. 5 (b)], the enhanced electric field extends 50 nm into the gaps between Au nano-triangles, much larger than the gap formed in nanoparticle-based substrates. Such large SERS-active zone makes this structure suitable for label-free direct SERS sensing of macromolecules such as proteins and DNAs. In addition, the properties of graphene make it possible to modulate SERS effects using the hybrid graphene/metallic nano-structures.

Conclusion

Au nano-triangle array-based SERS fiber probe is prepared. Effects of optical lens, slit width, fiber length, and array size on Raman signal intensity are investigated. Matching the NA of lens to the NA of fiber and matching of the slit width to the size of the enlarged fiber core image can help increasing the Raman signal. The Raman signal intensity appears to be independent of the fiber length up to several meters, but the S/N will decrease with fiber length. Size of SERS array coated on fiber facet is one primary factor accounting for the Raman signal loss, which is ultimately due to the laser power density decrease on the fiber end. SERS fiber probe with hybrid graphene/Au nano-array is found to be superior to the fiber probe with bare Au nano-array in terms of the sensitivity. The fabrication method proposed here can be used to further enhance the fiber probe spatial resolution.

Acknowledgements

This work is supported by FAME, one of six centers of STARnet, a Semiconductor Research Corporation program sponsored by MARCO and DARPA. Y. H. Xie acknowledges the support from Alexander von Humboldt Foundation Research Award.

References

[1] P. L. Stiles, J. A. Dieringer, N. C. Shah, R. P. Van Duyne, *Annu. Rev. Anal. Chem.* **2008**, *1*, 601.
[2] E. C. Le Ru, P. G. Etchegoin, *Annu. Rev. Phys. Chem.* **2012**, *63*, 65.
[3] M. Kahraman, I. Sur, M. Culha, *Anal. Chem.* **2010**, *82*, 7596.
[4] Z. Xie, S. Feng, P. Wang, L. Zhang, X. Ren, L. Cui, T. Zhai, J. Chen, Y. Wang, X. Wang, *Adv Opt Mater* **2015**, *3*, 1232.
[5] M. Xia, K. Qiao, Z. Cheng, Y.-H. Xie, *Appl Phys Express* **2016**, *9*, 065001.
[6] W. Xu, X. Ling, J. Xiao, M. S. Dresselhaus, J. Kong, H. Xu, Z. Liu, J. Zhang, *Proc. Natl. Acad. Sci.* **2012**, *109*, 9281.
[7] P. Wang, O. Liang, W. Zhang, T. Schroeder, Y. H. Xie, *Adv. Mater.* **2013**, *25*, 4918.

[8] X. Ling, W. Fang, Y.-H. Lee, P. T. Araujo, X. Zhang, J. F. Rodriguez-Nieva, Y. Lin, J. Zhang, J. Kong, M. S. Dresselhaus, *Nano Lett.* **2014**, *14*, 3033.
[9] W. Xu, N. Mao, J. Zhang, *Small* **2013**, *9*, 1206.
[10] X. Qian, X.-H. Peng, D. O. Ansari, Q. Yin-Goen, G. Z. Chen, D. M. Shin, L. Yang, A. N. Young, M. D. Wang, S. Nie, *Nat. Biotechnol.* **2008**, *26*, 83.
[11] A. Samanta, K. K. Maiti, K. S. Soh, X. Liao, M. Vendrell, U. Dinish, S. W. Yun, R. Bhuvaneswari, H. Kim, S. Rautela, *Angew. Chem., Int. Ed.* **2011**, *50*, 6089.
[12] H. Chu, Y. Liu, Y. Huang, Y. Zhao, *Opt. Express* **2007**, *15*, 12230.
[13] R. Gessner, P. Rösch, R. Petry, M. Schmitt, M. Strehle, W. Kiefer, J. Popp, *Analyst* **2004**, *129*, 1193.
[14] A. Foti, C. D'Andrea, F. Bonaccorso, M. Lanza, G. Calogero, E. Messina, O. M. Maragò, B. Fazio, P. G. Gucciardi, *Plasmonics* **2013**, *8*, 13.
[15] T. Liu, X. Xiao, P. Wang, L. Ji, C. Yang, *Chem Phys Lett* **2012**, *553*, 51.
[16] E. J. Smythe, M. D. Dickey, J. Bao, G. M. Whitesides, F. Capasso, *Nano Lett.* **2009**, *9*, 1132.
[17] S. Mondal, U. Rana, S. Malik, *ACS Appl. Mater. Interfaces* **2015**, *7*, 10457.
[18] J. Zhang, S. Chen, T. Gong, X. Zhang, Y. Zhu, *Plasmonics* **2015**, 1.
[19] J. Cao, D. Zhao, Q. Mao, *RSC Adv* **2015**, *5*, 99491.
[20] J. S. Daniels, N. Pourmand, *Electroanalysis* **2007**, *19*, 1239.
[21] M. Fan, P. Wang, C. Escobedo, D. Sinton, A. G. Brolo, *Lab Chip* **2012**, *12*, 1554.
[22] R. T. Kennedy, *Curr. Opin. Chem. Biol.* **2013**, *17*, 860.
[23] L. Siksou, P. Rostaing, J.-P. Lechaire, T. Boudier, T. Ohtsuka, A. Fejtová, H.-T. Kao, P. Greengard, E. D. Gundelfinger, A. Triller, *J. Neurosci.* **2007**, *27*, 6868.
[24] C. Kong Chong, C. Shen, Y. Fong, J. Zhu, F.-X. Yan, S. Brush, C. K. Mann, T. J. Vickers, *Vib Spectrosc* **1992**, *3*, 35.
[25] P. Wang, M. Xia, O. Liang, K. Sun, A. F. Cipriano, T. Schroeder, H. Liu, Y.-H. Xie, *Anal. Chem.* **2015**, *87*, 10255.
[26] X. Ling, L. Moura, M. A. Pimenta, J. Zhang, *J. Phys. Chem. C* **2012**, *116*, 25112.
[27] X. Ling, J. Zhang, *Small* **2010**, *6*, 2020.
[28] X. Ling, L. Xie, Y. Fang, H. Xu, H. Zhang, J. Kong, M. S. Dresselhaus, J. Zhang, Z. Liu, *Nano Lett.* **2009**, *10*, 553.
[29] K. Liu, J.-J. Zhang, F.-F. Cheng, T.-T. Zheng, C. Wang, J.-J. Zhu, *J. Mater. Chem.* **2011**, *21*, 12034.
[30] Y. Liu, D. Yu, C. Zeng, Z. Miao, L. Dai, *Langmuir* **2010**, *26*, 6158.
[31] Y.-K. Kim, M.-H. Kim, D.-H. Min, *Chem. Commun.* **2011**, *47*, 3195.

Supporting information

Additional supporting information may be found in the online version of this article at the publisher's web site.